Biosensors and Bioelectronics 144 (2019) 111575

Contents lists available at ScienceDirect

Biosensors and Bioelectronics

journal homepage: www.elsevier.com/locate/bios

A novel light-electricity sensing method for PCSK9 detection based on s-PdNFs with multifunctional property

Chengli Zhang[a,b,1], Junlin He[a,1], Jia Li[a], Yuan Zhou[a], Xiaoxue Fu[a], Yilin Zhao[c], Jun Chen[a], WeiRan Mao[a], Chao Yu[a,*,2]

[a] Institute of Life Science, College of Pharmacy and School of Public Health, Chongqing Medical University, Chongqing, 400016, PR China
[b] The First People's Hospital of Neijiang, Sichuan, 641000, PR China
[c] Department of Clinical Laboratory, Xi'an No. 4 Hospital, Guangren Hospital Affiliated to School of Medicine of Xi'an Jiaotong University, Xi'an, 710000, PR China

ARTICLE INFO

Keywords:
s-PdNFs
PCSK9
Light-electricity dual signal immunosensor
ECL-RET system
Catalysis

ABSTRACT

Amounts of studies show that proprotein convertase subtilisin/kexin type 9 (PCSK9) can increase the low-density lipoprotein cholesterol ((LDL-C), leading to the progression and development of atherosclerosis. Hence, design an effective method to detect serum PCSK9 is meaningful for the prevention, monitor and diagnosis of cardiovascular diseases. Here, we reported a dual-signal method for detecting PCSK9 using a signal label, sulphur-doped palladium nanoflowers (s-PdNFs), inspired by its multifunctional properties of quenching and catalysis, which would simultaneously achieve electrochemiluminescence (ECL) analysis and electrochemical detection. For the ECL analysis, s-PdNFs could effectively quench the ECL intensity of peroxydisulfate/oxygen ($S_2O_8^{2-}/O_2$) system via ECL resonance energy transfer (ECL-RET). Importantly, the donor-acceptor pair (s-PdNFs-$S_2O_8^{2-}$ pair) was firstly reported in the ECL-RET field. For the electrochemical detection, s-PdNFs with peroxidase-like activity, produce electric signals by catalyzing H_2O_2. Herein, a novel light-electricity dual signal immunosensor based on s-PdNFs was developed, and with a broad linear range of 5 fg mL^{-1} to 50 ng mL^{-1} (ECL channel) and 500 fg mL^{-1} to 50 ng mL^{-1} (electrochemical channel). Furthermore, the ECL channel and electrochemical channel can achieve the detection respectively which can meet different testing instruments. The two channels can also be combined to improve the accuracy of the detection. More importantly, the immunosensor realized the detection of PCSK9 in real serum samples demonstrated by good correlations with ELISA method. Our findings can promote the application of multifunctional materials in sensor and biomedicine field and provide a novel strategy for the detection of serum molecular.

1. Introduction

Atherosclerosis is a common cardiovascular disease with high risk of morbidity and mortality, characterized by raised low-density lipoprotein cholesterol (LDL-C). Recent studies reveal that proprotein convertase subtilisin/kexin type 9 (PCSK9) can promote LDL-C accumulation (Cui et al., 2010), and the inhibition of PCSK9 can reduce LDL-C levels in patients with cardiovascular high risk (Annemans et al., 2018). Hence, the detection of serum PCSK9 is necessary for the prevention, monitoring and diagnosis of cardiovascular diseases (Huijgen et al., 2012; Wang et al., 2015). Furthermore, accurate quantification of PCSK9 is beneficial to the guidance of clinical safe medication. Thus, it is imperative to construct an effective method to detect PCSK9.

Recently, electrochemical detection and electrochemiluminescence (ECL) analysis have been widely applied to detect serum markers, and as promising analytical methods because of their outstanding advantages, such as sensitivity, simplicity and fast response (Bai et al., 2017; Li et al., 2017a). Nevertheless, single signal output usually used in sensors analysis is difficult to ensure signal accuracy. Thus, some dual-signal sensors have been reported to analyze biological and chemical samples. For example, Wei's group constructed a dual-responsive electrochemical immunosensor for prostate specific antigen detection (Wei et al., 2017). Mak's group reported a dual-responsive for fluorescent immunoassays and colorimetric enzymatic bioassays (Lai et al., 2012). Inspired by above findings of dual-signal system, it can be drawn two main conclusions: 1. If the dual-signal could achieve the detection

* Corresponding author. Tel.: 86 023 68485378.
E-mail address: yuchaom@163.com (C. Yu).
[1] Junlin He and Chengli Zhang contributed equally to this work.
[2] Box 380#, College of Pharmacy, Chongqing Medical University, No.1 ,Yi Xue Yuan Road, Yuzhong district, Chongqing 400016, P. R. China.

https://doi.org/10.1016/j.bios.2019.111575
Received 21 June 2019; Received in revised form 29 July 2019; Accepted 5 August 2019
Available online 13 August 2019
0956-5663/

in different instruments, we could choose one of the instruments to detect targets according to the instrument condition. 2. The dual-signal can also be combined to judge the results to improve the accuracy of the detection (Wei et al., 2017). Considering the advantages of electrochemical, ECL and dual-signal sensor, we integrate the ECL analysis and electrochemical detection into a dual-signal sensor, which aims to construct a novel dual-signal immunosensor (light-electricity dual signal immunosensor) for PCSK9 detection. It's worth noting that the light-electricity dual signal immunosensor have not been reported for the analytical detection in sensors field.

A multifunctional nanomaterial is the key point in constructing a light-electricity dual signal immunosensor, which can change the light-electricity signal output. Studies show that sulphur-doped palladium is endowed various physicochemical properties due to its multivalence state with exceeding importance (Nandan and Nanda, 2017). The sulphur-doped palladium nanoflowers (s-PdNFs) with fascinating properties like high surface area and plenty of absorption/active sites in tiny space had been successfully synthesized according to previous work (Nandan and Nanda,2017). Importantly, we found that s-PdNFs not only effectively quenched the ECL intensity of peroxydisulfate/oxygen ($S_2O_8^{2-}/O_2$) system but also produced electric signal via catalyzing H_2O_2, which was firstly reported as the multifunctional nanomaterial. The multifunctional features of s-PdNFs could be employed as a signal label and provide great possibilities to construct a novel light-electricity dual signal immunosensor.

For the ECL analysis (light signal), we used the mechanism of electrochemiluminescence resonance energy transfer (ECL-RET). ECL-RET is based on the principle of nonradiative energy transfer phenomenon between a perfectly matched donor and acceptor pair (Babamiri et al., 2018; Ke et al., 2018). Due to non-excitation light source, non-interference scattered light and high sensitivity, ECL-RET has drawn wide concern in detecting different targets (He et al., 2013; Liu et al., 2015; Wu et al., 2014). However, some challenges are always exist in searching the corresponding donor-acceptor pair. One of the big challenges is the lack of donor-acceptor system with excellent spectrum overlap (Ma et al., 2016). Besides, the reported ECL-RET system is exhibited disadvantages more or less. For example, the luminol reagents need to keep in dark place, the quantum dots are usually poisonous and bad biocompatibility and the price of $Ru(bpy)_3^{2+}$ is expensive (Feng et al., 2016; Li et al., 2017b; Zhao et al., 2015a). Thus, efficient, nontoxic, cheapness and oversimplified ECL-RET system is in need of being exploited to supplement more types of donor-acceptor. As an ECL luminophore, the $S_2O_8^{2-}$ has attracted increasing attention in the construction of ECL sensor due to its fascinating merits of cheapness, availability and accessibility (E.P. Koval'chuk et al., 1999; Lei et al., 2015; VM. et al., 1982; Yao et al., 2008). But, scanty studies of $S_2O_8^{2-}/O_2$ ECL system are related to the ECL-RET capability. The main reason is lack of appropriate donor or acceptor with good spectrum overlap, which limits its application in ECL-RET field. Interestingly, s-PdNFs exhibited broad ultraviolet (UV) absorption spectra, making it easy to trigger the ECL-RET in $S_2O_8^{2-}/O_2$ system. Our work revealed that an ECL immunosensor was constructed for the first time based on ECL-RET process of s-PdNFs and $S_2O_8^{2-}/O_2$ system (ECL channel).

In terms of the electrochemical analysis (electricity signal), s-PdNFs had peroxidase-like activity that produces electrochemical signals by catalyzing H_2O_2, which was recorded by i-t curve. Herein, a novel electrochemical sensor (electrochemical channel), using s-PdNFs as signal tag and amperometric i-t curve as signal, was constructed for the first time. In conclusion, the prepared s-PdNFs with strong quenching for ECL intensity and suitable catalysis property could break the bottleneck of the foundation and application of the light-electricity dual signal sensor.

In the present work, a “sandwich” type light-electricity dual signal immunosensor was firstly designed for PCSK9 detection (as shown in Scheme 1). The s-PdNFs played the roles of quenching the ECL signal of $S_2O_8^{2-}/O_2$ system by the mechanism of ECL-RET and producing electrochemical current response by catalyzing H_2O_2. First, because of the excellent conductivity, large specific surface area and good biocompatibility (Liu et al., 2013; Wang et al., 2014b), gold nanoparticles (AuNPs) were electrodeposited on a glassy carbon electrode (GCE) to improve the ECL intensity and current response. Then, the primary antibody (Ab_1) was loaded on the modified electrode surface, forming a sensing interface to PCSK9 antigen. In the presence of target PCSK9, the s-PdNFs labeled secondary antibody (s-PdNFs-Ab_2) could be immobilized on the fabricated immunosensor, a decreased ECL response was obtained in $K_2S_2O_8$ solution or an increased current response was recorded in PBS solution by adding H_2O_2. This work has the following four major advantages: (1) s-PdNFs was prepared with a simple, single-pot, one-step and surfactant free method. (2) s-PdNFs was reported as the multifunctional nanomaterial for the first time that it not only effectively quenched the ECL intensity of $S_2O_8^{2-}/O_2$, but also produced electrochemical signals by catalyzing H_2O_2. (3) A novel donor-acceptor pair (s-PdNFs-$S_2O_8^{2-}$ pair) was developed, which has not been reported previously. (4) A light-electricity dual signal immunosensor was fabricated successfully for the first time, which can meet different testing instruments. Moreover, the two signal channels can also be combined to judge the detection result to improve the accuracy of the detection.

2. Experience section

2.1. Chemicals and apparatus

The chemicals and apparatus are showed in detail in the Supporting information (S1).

2.2. Synthesis of sulphur-doped Pd nanoflowers (s-PdNFs) and Ab_2 bioconjugate

The s-PdNFs was synthesized by the oxidative polymerization of methylene blue (M.B.) using sodium tetrachloropalladate (Na_2PdCl_4) as oxidant (Nandan and Nanda, 2017). Briefly, Na_2PdCl_4, (28.5 mM, 3 mL) and M.B. (0.1 mM, 3 mL) were mixed with stirring. Then the mixture solution was reacted at 90 °C with slightly stirring. After being centrifuged and washed, the s-PdNFs was dispersed in 1 mL ultrapure water for further use.

Then, the Ab_2 of PCSK9 of 200 μL could be immobilized on the surface of s-PdNFs after stirring at 4 °C for 24 h. Afterwards, in order to block nonspecific adsorption, BSA was added into above mixture. After washing, the bioconjugate (s-PdNF-Ab_2) were dispersed in ultrapure water and stored at 4 °C prior to use.

2.3. Fabrication of the light-electricity dual signal immunosensor

The preparation procedure of the immunosensor was displayed in Scheme 1. Prior to modification, a mirror-like glassy carbon electrode (GCE) surface was acquired by being polished with 0.3 and 0.05 μm alumina powders. The polished GCE was washed with Milli-Q water, alcohol and Milli-Q water. Subsequently, AuNPs were electrodeposited on the GCE surface under the potential of −0.2 V for 30 s in a gold (III) chloride trihydrate ($HAuCl_3{\cdot}3H_2O$, 1 %, w/v) solution. Then, 10 μL of the Ab_1 (Dilute 100 times) was immobilized on GCE/AuNPs at 4 °C overnight. After washed, 6 μL of bovine serum albumin (BSA) solution was coated on the GCE/AuNPs/Ab_1 for 30 min at room temperature. Lastly, these electrodes were washed to eliminate unbound BSA.

2.4. The measurement of the light-electricity dual signal immunosensor

After the immunosensor (GCE/AuNPs/Ab_1/BSA) was incubated with 10 μL of multiple concentrations of PCSK9 for 2 h at 37 °C, it was further incubated with 10 μL of s-PdNFs-Ab_2 at 37 °C for 2 h. The ECL measurement was performed in 8 mL PBS (pH 8.0) containing 0.16 M $K_2S_2O_8$ with a scanned potential from 0 to −2.5 V, and the scan rate

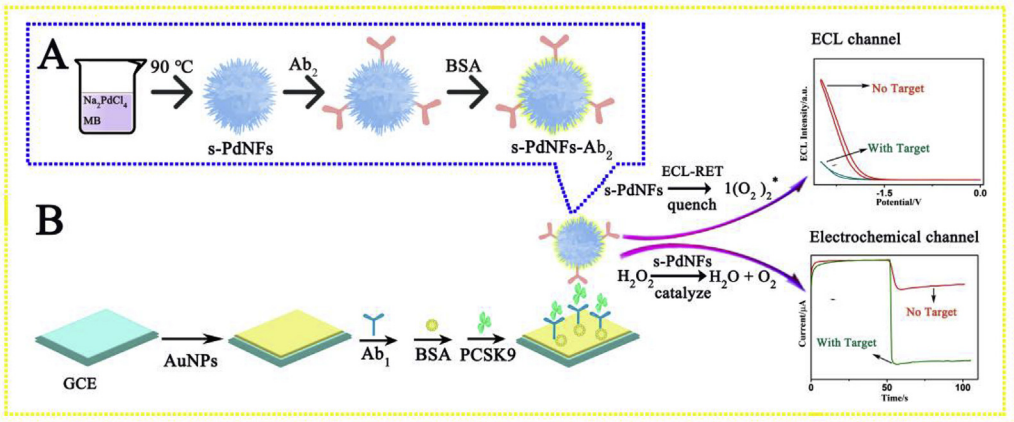

Scheme 1. (A) The preparation process of s-PdNFs-Ab_2. (B) Schematic illustration of the light-electricity dual signal immunosensor.

was 400 mV s^{-1}. The voltage of the photomultiplier tube (PMT) was 800 V. The electrochemical signal of i-t curve was recorded at −0.4 V in phosphate buffered saline (5 mL, 0.1 M PBS, pH 7.4). When the background current was stable, the current changes were recorded by adding 20 μL of H_2O_2 (2.0 mol L^{-1}) to the PBS.

3. Results and discussion

3.1. Characterization of s-PdNFs

In the synthesis process of s-PdNF, time plays a key role. First, Fig. S1A showed the photograph of s-PdNFs products in the different synthesis time. Second, transmission electron microscopy (TEM) was used to further characterize the size and morphology of the as-prepared s-PdNF nanomaterials. There were few products, while the synthesis condition of s-PdNFs was at 1.5 h for 90 °C (a in Fig. S1A). When the time (1.5 h) is replaced by 6 h, there were some products (b in Fig. S1A), but the size of s-PdNFs was greatly inhomogenous (Fig. S1B). However, when the reaction was at 1.5 h for 90 °C, followed by overnight stirring at room temperature, the product still existed (c in Fig. S1A) and the particles of s-PdNFs were of 30 nm in size and had a regular and uniform size (Fig. S1C). Thus, the optimum condition (mixing M.B. and Na_2PdCl_4 at 1.5 h for 90 °C, followed by stirring overnight at room temperature) was applied throughout the synthesis process. Besides, when s-PdNFs was stored at 4 °C for 9 months, its morphology did not change (Fig. S1D). The results showed that s-PdNFs was prepared successfully and had good stability.

The high resolution TEM and field emission scanning electron microscopy (FE-SEM) were also used to further characterize the size and structure of the as-prepared s-PdNF nanomaterials. As shown in Fig. 1A and Fig. 1B, the s-PdNFs displayed hydrangea-like structure and suggested that the single s-PdNF was composed of many small particles connected to each other. The primary particles were of 3–5 nm in size and these nanoparticles were interconnected to form hydrangea-like structures (Fig. 1C). Besides, the FE-SEM images further indicated that the s-PdNFs with a smooth surface and were of 30 nm in size (Fig. 1D).

In order to confirm the elements valence of s-PdNFs, a X-ray photoelectron spectroscopy (XPS) characterization was displayed in Fig. 1E. The fitted core spectrum of Pd 3d showed peaks at 335.6 eV, 337.38 eV and 342.78 eV corresponding to Pd^0, Pd^{2+} and high-valency palladium ions, respectively (Sadhanala et al., 2016; Sun et al., 2011). The peaks around 163 eV and 167 eV indicate the S^{2-} and S^{6-} states (Xu et al.; Zhang et al., 2015). The spectrum of Pd3d and S2p were displayed in Figs. 1F–2G. The XPS results verified that the elements valence of Pd and S were multivalent. The multivalent state may be the key factor for its multifunction.

These above results indicated that the successful preparation of s-PdNFs. In addition, a further testimony of the formation of s-PdNFs and s-PdNFs-Ab_2 through ζ-potential, UV-absorption spectra and energy dispersive X ray spectroscopy are displayed in Supporting information. The SEM image and description of electrodeposited AuNPs are shown in Supporting information.

3.2. Electrochemical impedance spectroscopy and cyclic voltammetry characterization of the light-electricity dual signal immunosensor construction

The description was displayed in Supporting information.

3.3. The ECL mechanism of the diffirent system

In 1982, Koval'chuk first reported the ECL phenomenon of $S_2O_8^{2-}$ solution (Koval'chuk et al., 1999). The ECL system of $S_2O_8^{2-}$/oxygen ($S_2O_8^{2-}/O_2$) had attracted increasing interest in developing ECL sensor, because of its merits of simplicity, cheapness and accessibility (Dai et al., 2014; Wang et al., 2014a). The ECL mechanisms of $S_2O_8^{2-}/O_2$ system are follows:

$$S_2O_8^{2-} + e^- \rightarrow SO_4^{\bullet -} + SO_4^{2-}$$

$$SO_4^{\bullet -} + H_2O \rightarrow HO^{\bullet} + HSO_4^-$$

$$3HO^{\bullet} \rightarrow HOO^{\bullet} + H_2O$$

$$O_2 + H_2O + e^- \rightarrow HOO^{\bullet} + HO^-$$

$$2SO_4^{\bullet -} + 2HOO^{\bullet} \rightarrow 2HSO_4^- + 1(O_2)_2 *$$

$$1(O_2)_2 * \rightarrow 2^3 O_2 + h\nu$$

However, the ECL response of $S_2O_8^{2-}/O_2$ system showed weak sensitivity without adding enhancers (curve a in Fig. 2A), which was consistent with the previous report (Zhao et al., 2015b). Thus, as can be seen in Fig. 2A (curve b), the AuNPs layer achieved the "signal amplify" state in this work. Specifically, the phenomenon could be observed that the GCE/AuNPs surface gave about 7 times higher ECL intensity in the $S_2O_8^{2-}$ solution than that of a bare GCE (curve b vs. a), which indicated that AuNPs could enhance the ECL emission of $S_2O_8^{2-}/O_2$ system (Zhao et al., 2015b). When GCE/AuNPs was incubated with Ab_1, BSA and PCSK9, respectively, the ECL intensity was successively decreased (curve c-e) due to non-conductive protein hindering electron transfer. Finally, the "signal quenching" state (curve f) was obtained by incubating with s-PdNFs-Ab_2 on GCE/AuNPs/Ab_1/BSA/PCSK9, which has the high quenching rate about 85 % on the basis of the ratio of the quenched intensity and the initial intensity (Cao et al., 2006; Chen et al., 2010). The result demonstrated that s-PdNFs could effectively quench the ECL emission of $S_2O_8^{2-}/O_2$ system.

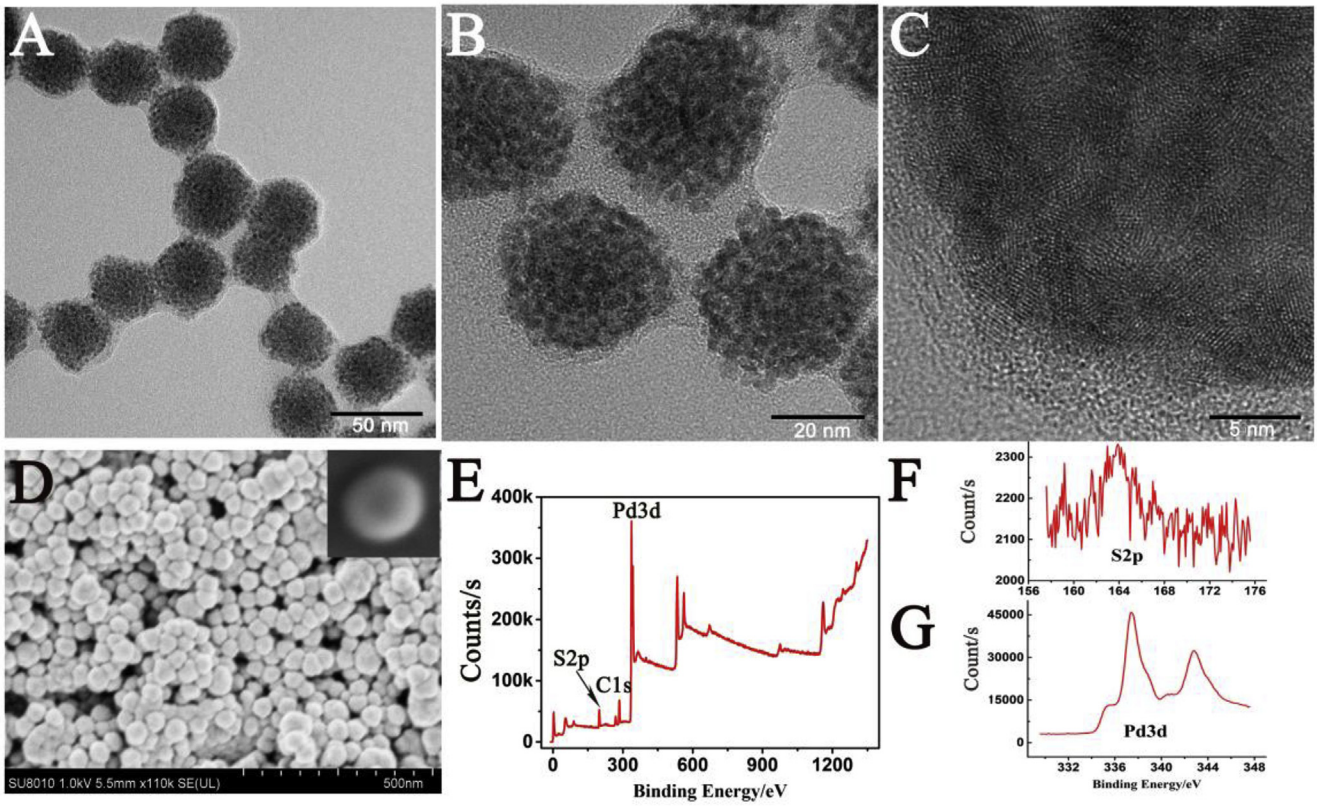

Fig. 1. (A), (B) and (C) The high resolution TEM image of s-PdNF; (D) FE-SEM images of s-PdNF; (E) The XPS spectrum of s-PdNF, (F) S2p in s-PdNF and (G) Pd3d in s-PdNF.

The ECL spectrum was applied to identify the ECL signal source in the $S_2O_8^{2-}/O_2$ system. As shown in Fig. 2B, the spectrum of the bare GCE (curve a) and the GCE/AuNPs (curve b) in $S_2O_8^{2-}$ solution displayed the identical emission peak at 600 nm, confirming that the luminophore was the $^1(O_2)_2$* (Yang et al., 2018) and AuNPs acted as an accelerator in $S_2O_8^{2-}/O_2$ system.

To further clarify the ECL enhanced mechanism in the $S_2O_8^{2-}/O_2$ system, the cyclic voltammetry (CV) curves of the bare GCE (curve a&b) and the GCE/AuNPs (curve c) were acquired in $S_2O_8^{2-}$ solution (Fig. 2C). Reaction solution was filled with nitrogen to remove dissolved oxygen (curve a). The bare GCE exhibited a reduction peak at −1.51 V regardless of the presence of oxygen (curve a&b), which revealed that the strong oxidant of $SO_4^{\bullet-}$ was produced by electrochemical reduction of $S_2O_8^{2-}$. The reduction peak of curve b was higher than curve a. The reason may be that $HOO^{\bullet}$ is decreased without oxygen, which resulting in decreased current. Nevertheless, the CV curve of GCE/AuNPs showed a positive shift (−0.70 V) in the reduction peak potential and an increased in peak current (curve c) in comparison that of curve b. Besides, no new redox peaks presented in curve c. The result demonstrated that AuNPs could accelerate the reduction of $S_2O_8^{2-}$ due to the excellent conductivity of AuNPs (Zhao et al., 2015b) and there were no new redox reactions happened between AuNPs and $S_2O_8^{2-}/O_2$ system.

The ECL quenched behavior of s-PdNFs was further investigated in Fig. 2D. $S_2O_8^{2-}/O_2$ system could generate negligible ECL and AuNPs can boost the ECL intensity of $^1(O_2)_2$* (curve a and c), but the ECL emission of $^1(O_2)_2$* was effectively quenched once s-PdNFs solution were brought into the reaction solution of GCE or GCE/AuNPs (curve b and d). The decreased ECL intensity also confirmed that s-PdNFs could quench the ECL emission of $^1(O_2)_2$*. And with regard to the quenched mechanism of this system, ECL spectrum of $S_2O_8^{2-}/O_2$ system and UV-vis absorption spectrum of s-PdNFs have been explored. As seen from Fig. 2E, there was a good spectra overlaps between the ECL spectra of $S_2O_8^{2-}/O_2^-$ system (500–625 nm, curve a) and the UV-vis absorption spectra of s-PdNFs (400–700 nm, curve b), which mean that the overlap between emission spectra of $S_2O_8^{2-}/O_2$ system (donor) and absorption spectra of s-PdNFs (acceptor) enabled the happening of ECL-RET procedure (Ma et al., 2016).

Besides, to further investigate the quenched mechanism of this system, the CV responses of the four different solutions were also presented in Fig. 2F. Without redox peak appeared in the CV curves of GCE and GCE/AuNPs in s-PdNFs solution (Fig. 2F, curve a and c). After $K_2S_2O_8$ was added in s-PdNFs solution, a reduction peak of $S_2O_8^{2-}$ was appeared in the CV curves of GCE and GCE/AuNPs. It suggested that when voltage was applied, s-PdNFs did not react by themselves, and s-PdNFs did not react with AuNPs and $S_2O_8^{2-}/O_2$ system. Thus, the quenched mechanism of this system may not involve in redox reaction.

s-PdNFs-Ab$_2$ in 0.12 M $K_2S_2O_8$ solution, respectively. The inset of (A): ECL-time profiles of curve a and curve b. (scan range: 0 to −2.5 V, *vs* Ag/AgCl); (B) Normalized ECL spectrum of (a) bare GCE and (b) GCE/AuNPs in 0.12 M $K_2S_2O_8$ solution. The inset of (B): Individual figure of curve b (scan range: 0 to −2.5 V); (C) CV responses of (a) bare GCE in $K_2S_2O_8$ solution withiout O_2, (b) bare GCE in $K_2S_2O_8$ solution and (c) GCE/AuNPs in $K_2S_2O_8$ solution.The inset of (C): Individual figure of curve a. (D) ECL-potential profiles: (a) bare GCE + 0.12 M $K_2S_2O_8$ solution, (b) bare GCE + 0.12 M $K_2S_2O_8$ solution + s-PdNFs solution. (c) GCE/AuNPs + 0.12 M $K_2S_2O_8$ solution, (d) GCE/AuNPs + 0.12 M $K_2S_2O_8$ solution + s-PdNFs solution; (E) ECL spectrum of $S_2O_8^{2-}/O_2^-$ system and UV-vis spectrum of s-PdNFs (curve a and curve b, respectively); (F) CV responses of (a) bare GCE + s-PdNFs solution, (b) bare GCE + $K_2S_2O_8$ solution + s-PdNFs solution. (c) GCE/AuNPs + s-PdNFs solution, (d) GCE/AuNPs + $K_2S_2O_8$ solution + s-PdNFs solution.

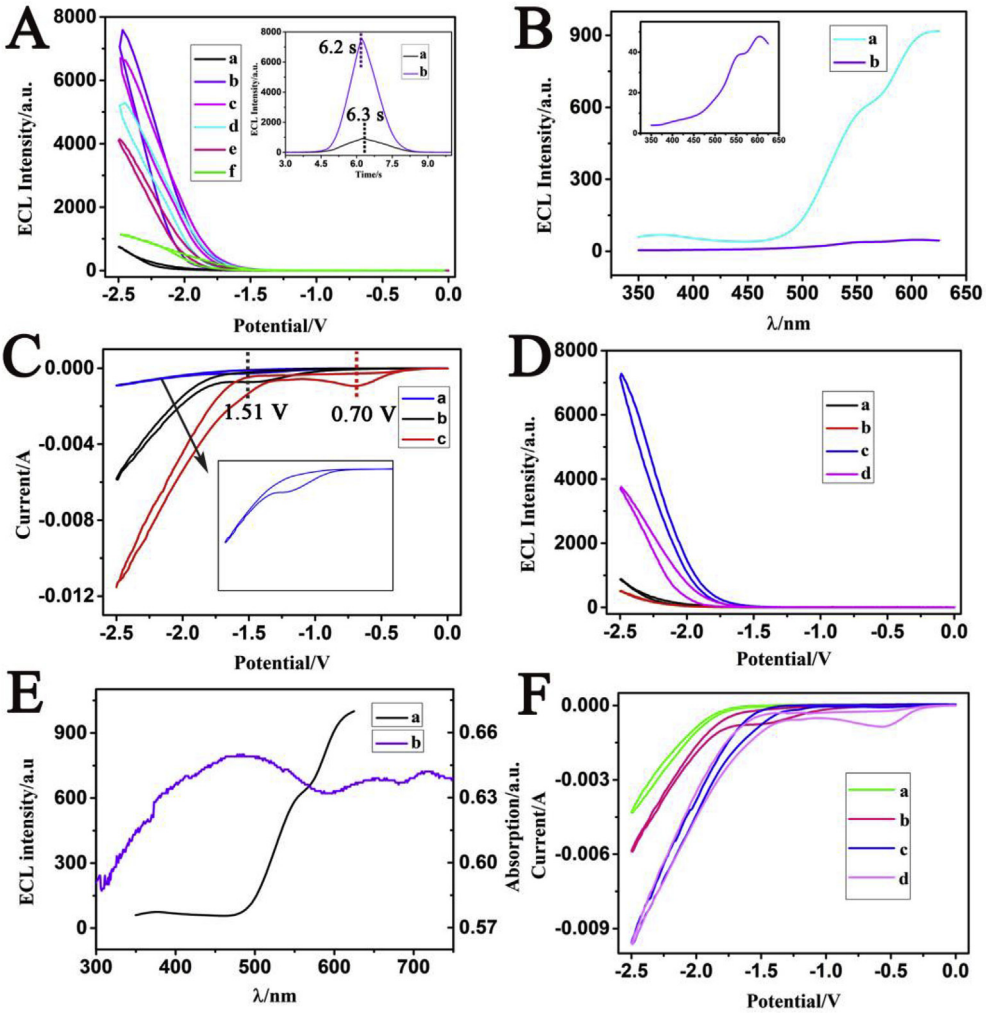

Fig. 2. (A) ECL-potential profiles: (a) bare GCE, (b) GCE/AuNPs (c) GCE/AuNPs/Ab_1, (d) GCE/AuNPs/Ab_1/BSA (e) GCE/AuNPs/Ab_1/BSA/PCSK9 and (f) GCE/AuNPs/Ab_1/BSA/PCSK9/.

3.4. Optimizations of the experimental conditions

The optimizations of the experimental conditions are described in detail in the Supporting information.

3.5. Analytical performance of the light-electricity dual signal immunosensor

To explore the performance of the prepared light-electricity dual signal immunosensor, different concentrations of PCSK9 were determinated under the optimal conditions. On the one hand, the proposed ECL channel was applied to detect a series of concentrations of PCSK9. As presented in Fig. 3A, the ECL intensity decreased accordingly with the augment of PCSK9 concentration. As the concentration of PCSK9 increased, the amount of s-PdNF-Ab_2 captured on the electrode surface was increased, which can strongly quench the ECL emission of $^1(O_2)_2$*. The ECL intensity exhibited a good linear to the logarithm of the target concentration in the range of 5 fg mL^{-1} to 50 ng mL^{-1} with the detection limit of 1.67 fg mL^{-1} (S/N = 3). The linear regression equation was $Y = -342.56 \times X + 3342.98$ (Fig. 3B). The results indicated that using s-PdNF-Ab_2 as the energy acceptor could efficiently quench the ECL response of $K_2S_2O_8$ donor and sensitively detect PCSK9 in the proposed ECL channel. On the other hand, the performance of electrochemical channel was explored. The amperometric i-t curve was recorded in 0.1 M PBS buffer (pH = 7.4) with 20 μL H_2O_2 and the current values are shown in Fig. 3C. The current response increased gradually with the increase of PCSK9 concentration from 500 fg mL^{-1} to 50 ng mL^{-1} (Fig. 3C). As seen in Fig. 3D, the linear regression equation is $Y = 10.38 \times X + 14.11$ and the correlation coefficient is 0.9984. The limit of detection (S/N = 3) is 166.67 fg mL^{-1}, indicating that using s-PdNF-Ab_2 as the redox probe and catalyst could detect PCSK9 with good sensitivity. Compared to other methods, the proposed method could identify PCSK9 with a broad linear range and a lower detection limit (Table S1).

To evaluate the specificity of the fabricated immunosensor, PCSK9, mixtures and nonspecific interferences, including dopamine (DA), BSA, glucose (Glu) and L-cysteine (L-Cys) were tested, and the results are shown in Fig. 4A. There existed a low current value due to the PCSK9. Moreover, the detection for PCSK9 (2.5 ng mL^{-1}) has not been effected by the high concentrations of disturbance components. These results revealed the good specificity of the proposed immunosensor. The stability of the ECL responses of this proposed immunosensor is demonstrated for PCSK9. As shown in Fig. 4B, the ECL intensities showed relative stable values under continuous CV scanning for 10 cycles. The reproducibility of the immunosensor was also examined by detecting the same PCSK9 concentration on the different electrodes (Fig. 4C). The RSD of inter-assay was 0.85 %, and the RSD of intra-assay value was 1.61 %. Thus, the proposed immunosensor had an acceptable reproducibility.

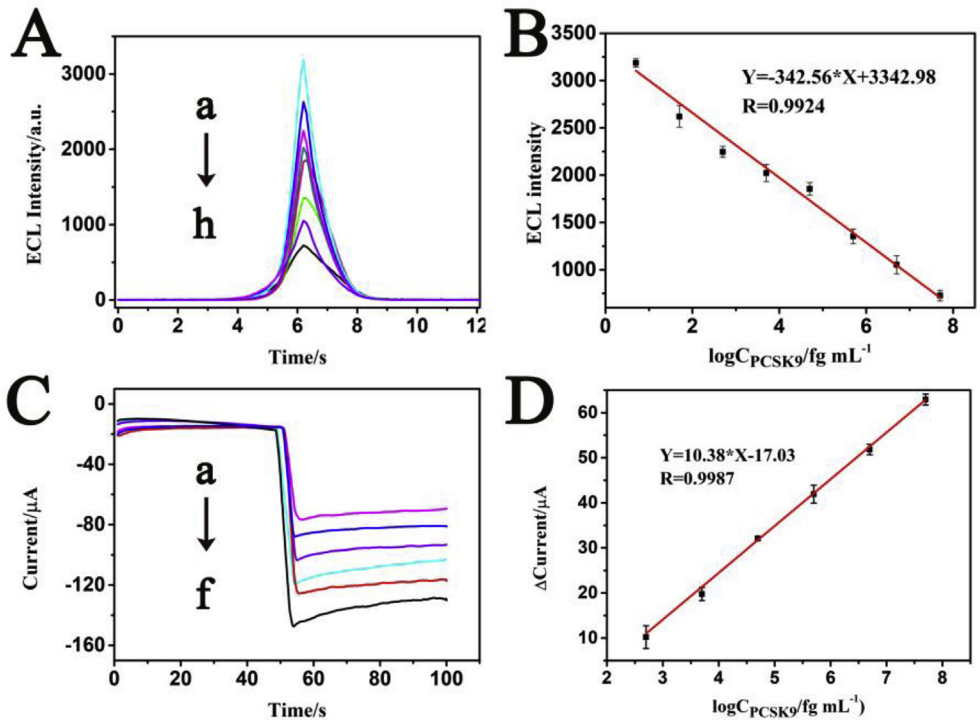

Fig. 3. (A) ECL responses of the light-electricity dual signal immunosensor (ECL channel) under optimized condition in different concentrations of PCSK9: (a–h: 5 fg mL^{-1}, 50 fg mL^{-1}, 500 fg mL^{-1}, 5 pg mL^{-1}, 50 pg mL^{-1}, 500 pg mL^{-1}, 5 ng mL^{-1}, 50 ng mL^{-1}). (B) The calibration plot of the ECL channel for various concentrations of PCSK9 (n = 3). (C) The i-t curve signals of the light-electricity dual signal immunosensor (electrochemical channel) for the detection of various concentrations of PCSK9 (a–f: 500 fg mL^{-1}, 5 pg mL^{-1}, 50 pg mL^{-1}, 500 pg mL^{-1}, 5 ng mL^{-1}, 50 ng mL^{-1}). (D) The calibration plot of the electrochemical channel for various concentrations of PCSK9 (n = 3).

3.6. Analytical application of the immunosensor

To validate the potential of the light-electricity dual signal immunosensor in clinical applications, various analyte concentrations (500 pg, 1 ng and 10 ng) were spiked into human serum samples, which were diluted 20-fold. The data are listed in Table S2. The recovery rates fluctuated from 92 % to 104.2 % (ECL channel) and 92 %–96.9 % (electrochemical channel). The ranges of all RSDs were less than 5 %. These results showed the feasibility of the immunosensor in clinical applications.

3.7. Detection of PCSK9 in real samples

To further explore the reliability of the prepared immunosensor, human serum samples with different concentration LDL were detected by using the developed method and ELISA method. As shown in Table 1, the relative errors between the two methods were 2.21–13.07 % (electrochemical channel) and 0.25–8.40 % (ECL channel). Besides, as shown in Fig. S5, the concentrations of PCSK9 were significant difference ($P < 0.05$) between low concentration LDL (< 3.36) and high concentration LDL human serum samples (> 3.36). These results indicated that the increased PCSK9 can increase the LDL levels. These results verified that the immunosensor had good reliability to detect of PCSK9 in real samples.

4. Conclusion

In conclusion, a multifunctional s-PdNF was prepared with a simple, one-step and surfactant free method. Our results demonstrated that the s-PdNF could be applied to fabricate a light-electricity dual signal immunosensor for the detection of PCSK9. The developed light-electricity dual signal immunosensor has shown high sensitivity, good selectivity and broad linear ranges (ECL channel: 5 fg mL^{-1} to 50 ng mL^{-1}; electrochemical channel: 500 fg mL^{-1} to 50 ng mL^{-1}). The immunosensor realized the detection of PCSK9 in real serum sample demonstrated by good correlations with ELISA method. Moreover, a novel donor-acceptor pair (s-PdNFs-$S_2O_8^{2-}$ pair) was reported, which has not been reported previously. The s-PdNFs-$S_2O_8^{2-}$ pair could broad the usage of ECL-RET to detect various targets. Besides, the s-PdNF could be potentially applied to other filed, such chip systems, drug delivery and photoluminescence. Finally, we can choose one of the two signals of immunosensor to achieve the target detection according to the condition of the instrument. Moreover, the two signal channels can also be combined to judge the detection result to improve the accuracy of the

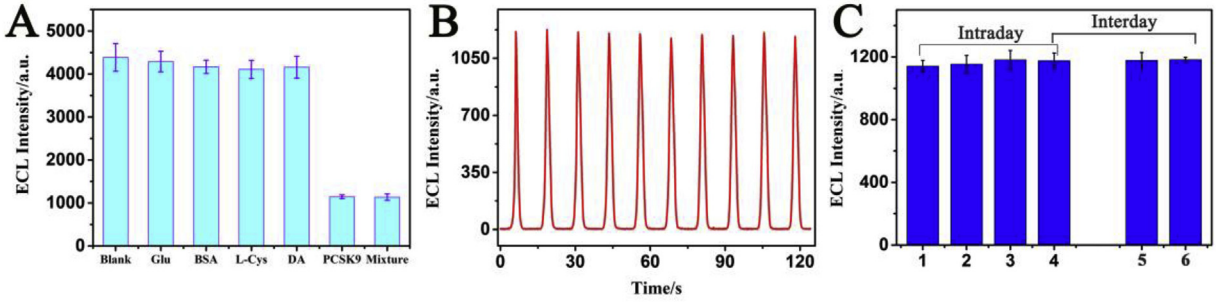

Fig. 4. (A) Specificity of the ECLimmunosensor towards: zero analyte; 1 μg mL^{-1} of Glu; 1 μg mL^{-1} of BSA; 1 μg mL^{-1} of L-Cys; 1 μg mL^{-1} of DA; 2.5 ng mL^{-1} of PCSK9 and the mixture consisted of PCSK9, Glu, BSA, DA and L-Cys. (B) Stability of the ECL under a continuous cyclic potential scan for the detection of 2.5 ng $mL^{-1}$of PCSK9. (C) Reproducibility of different electrodes modified with 2.5 ng mL^{-1} PCSK9.

Table 1
Detection of PCSK9 in human serum (n = 3) using the proposed method and ELISA.

Sample	LDL	This method/ electrochemical channel (ng mL^{-1})	This method/ ECL channel (ng mL^{-1})	ELISA (ng mL^{-1})	[a] Relative error (%)	[b] Relative error (%)
1	4.42	640.93	596.69	622.10	3.03	4.08
2	4.37	513.42	573.11	579.75	11.44	1.15
3	4.33	732.17	754.96	709.29	3.23	6.44
4	4.21	524.93	494.32	512.07	2.51	3.47
5	4.15	573.64	510.19	508.91	12.72	0.25
6	4.16	469.82	533.69	525.39	10.58	1.58
7	4.13	573.64	535.85	536.68	6.89	0.15
8	3.98	491.14	468.45	511.17	3.92	8.35
9	3.76	368.10	341.55	342.70	7.41	0.33
10	2.93	368.10	423.52	398.62	7.66	6.24
11	2.72	459.52	518.14	484.28	5.11	6.99
12	2.48	294.87	317.21	339.20	13.07	6.48
13	2.36	459.52	456.02	448.28	2.51	1.73
14	1.65	480.36	449.93	491.20	2.21	8.40
15	1.05	459.52	471.60	440.75	4.26	7.00

[a] The Relative error was calculated between electrochemical channel and ELISA.
[b] The Relative error was calculated between ECL channel and ELISA.

detection.

CRediT authorship contribution statement

Chengli Zhang: Writing - original draft, Formal analysis. **Junlin He:** Formal analysis, Writing - original draft. **Jia Li:** Formal analysis. **Yuan Zhou:** Validation. **Xiaoxue Fu:** Validation. **Yilin Zhao:** Formal analysis, Writing - review & editing. **Jun Chen:** Formal analysis, Writing - review & editing. **WeiRan Mao:** Writing - review & editing. **Chao Yu:** Formal analysis.

Acknowledgements

We are grateful for the financial support from the National Nature Science Foundation of China (No. 81370403), Chongqing foundation and advanced research project (No. CSTC2015jcyjBX0053), Chongqing precision medical key technology research and development and demonstration projects (cstc2016shms-ztzx0042), Chongqing Graduate Scientific Research Innovation Project (No.CYS17159) and Chongqing medical university scientific research cultivating fund (No.201414).

Appendix A. Supplementary data

Supplementary data to this article can be found online at https://doi.org/10.1016/j.bios.2019.111575.

References

Annemans, L., Packard, C.J., Briggs, A., Ray, K.K., 2018. Eur. Heart J. 39, 2546–2550.
Babamiri, B., Salimi, A., Hallaj, R., 2018. Biosens. Bioelectron. 102, 328–335.
Bai, L., Chen, Y., Bai, Y., Chen, Y., Zhou, J., Huang, A., 2017. Biomaterials 133, 11–19.
Cao, W., Ferrance, J.P., Demas, J., Landers, J.P., 2006. J. Am. Chem. Soc. 128, 7572–7578.
Chen, L., Cai, Q., Luo, F., Chen, X., Zhu, X., Qiu, B., Lin, Z., Chen, G., 2010. Chem. Commun. 46, 7751–7753.
Cui, Q., Ju, X., Yang, T., Zhang, M., Tang, W., Chen, Q., Hu, Y., Haas, J.V., Troutt, J.S., Pickard, R.T., Darling, R., Konrad, R.J., Zhou, H., Cao, G., 2010. Atherosclerosis 213, 632–636.
Dai, H., Xu, G., Zhang, S., Gong, L., Li, X., Yang, C., Lin, Y., Chen, J., Chen, G., 2014. Biosens. Bioelectron. 61, 575–578.
Feng, Y., Dai, C., Lei, J., Ju, H., Cheng, Y., 2016. Anal. Chem. 88, 845–850.
He, L.J., Wu, M.S., Xu, J.J., Chen, H.Y., 2013. Chem. Commun. 49, 1539–1541.
Huijgen, R., Boekholdt, S.M., Arsenault, B.J., Bao, W., Davaine, J.M., Tabet, F., Petrides, F., Rye, K.A., DeMicco, D.A., Barter, P.J., Kastelein, J.J., Lambert, G., 2012. J. Am. Coll. Cardiol. 59, 1778–1784.
Ke, H., Sha, H., Wang, Y., Guo, W., Zhang, X., Wang, Z., Huang, C., Jia, N., 2018. Biosens. Bioelectron. 100, 266–273.
Koval'chuk, E.P., Reshetnyak, O.V., Chernyak, A.O., Kovalyshyn, Y.S., 1999. Electrochim. Acta 44, 4079–4086.
Lai, K.K., Renneberg, R., Mak, W.C., 2012. Biosens. Bioelectron. 32, 169–176.
Lei, Y.M., Huang, W.X., Zhao, M., Chai, Y.Q., Yuan, R., Zhuo, Y., 2015. Anal. Chem. 87, 7787–7794.
Li, L., Chen, Y., Zhu, J.J., 2017a. Anal. Chem. 89, 358–371.
Li, Z., Lin, Z., Wu, X., Chen, H., Chai, Y., Yuan, R., 2017b. Anal. Chem. 89, 6029–6035.
Liu, X., Zhang, J., Liu, S., Zhang, Q., Liu, X., Wong, D.K., 2013. Anal. Chem. 85, 4350–4356.
Liu, Z., Qi, W., Xu, G., 2015. Chem. Soc. Rev. 44, 3117–3142.
Ma, H., Li, X., Yan, T., Li, Y., Liu, H., Zhang, Y., Wu, D., Du, B., Wei, Q., 2016. ACS Appl. Mater. Interfaces 8, 10121–10127.
Nandan, R., Nanda, K.K., 2017. Nanoscale 9, 12628–12636.
Sadhanala, H.K., Nandan, R., Nanda, K.K., 2016. Green Chem. 18, 2115–2121.
Sun, S., Zhang, G., Geng, D., Chen, Y., Li, R., Cai, M., Sun, X., 2011. Angew Chem. Int. Ed. Engl. 50, 422–426.
Wang, H., Bai, L., Chai, Y., Yuan, R., 2014a. Small 10, 1857–1865.
Wang, Y., Li, X., Cao, W., Li, Y., Li, H., Du, B., Wei, Q., 2014b. Biosens. Bioelectron. 61, 618–624.
Wang, Y., Wang, W., Yu, L., Tu, L., Feng, Y., Klein, T., Wang, J.P., 2015. Biosens. Bioelectron. 70, 61–68.
Wei, Y., Li, X., Sun, X., Ma, H., Zhang, Y., Wei, Q., 2017. Biosens. Bioelectron. 94, 141–147.
Wu, M.S., He, L.J., Xu, J.J., Chen, H.Y., 2014. Anal. Chem. 86, 4559–4565.
Xu, W., Ni, J., Zhang, Q., Feng, F., Xiang, Y., Li, X., J. Mater. Chem. 1, 12811-12817.
Yang, X., Yu, Y.Q., Peng, L.Z., Lei, Y.M., Chai, Y.Q., Yuan, R., Zhuo, Y., 2018. Anal. Chem. 90, 3995–4002.
Yao, W., Wang, L., Wang, H., Zhang, X., 2008. Electrochim. Acta 54, 733–737.
Zhang, Q., Feng, F., Su, C., Xu, W., Ma, L., Lu, C., Li, X., 2015. RSC Adv. 5, 66278–66285.
Zhao, H.F., Liang, R.P., Wang, J.W., Qiu, J.D., 2015a. Chem. Commun. 51, 12669–12672.
Zhao, M., Zhuo, Y., Chai, Y.Q., Yuan, R., 2015b. Biomaterials 52, 476–483.